Demonstration of Wire Bondless Silicon Carbide Power Module with Integrated LTCC Jet Impingement Cooler

Hao Chen
Electrical Engineering
University of Arkansas
Fayetteville, AR, USA
hc021@uark.edu

Tiwei Wei
Mechanical Engineering
Stanford University
Stanford, CA, USA
tiwei32@stanford.edu

Xiaoling Li
Electrical Engineering
University of Arkansas
Fayetteville, AR, USA
xl036@uark.edu

Yuxiang Chen
Electrical Engineering
University of Arkansas
Fayetteville, AR, USA
yc041@uark.edu

Yujui Lin
Mechanical Engineering
Stanford University
Stanford, CA, USA
yujuilin@stanford.edu

Sudharsan Chinnaiyan
Electrical Engineering
University of Arkansas
Fayetteville, AR, USA
schinnai@uark.edu

Mehdi Asheghi
Mechanical Engineering
Stanford University
Stanford, CA, USA
masheghi@stanford.edu

H. Alan Mantooth
Electrical Engineering
University of Arkansas
Fayetteville, AR, USA
mantooth@uark.edu

2022 IEEE Energy Conversion Congress and Exposition (ECCE) | 978-1-7281-9387-8/22/$31.00 ©2022 IEEE | DOI: 10.1109/ECCE50734.2022.9947694

***Abstract*—As wide-band-gap silicon carbide (SiC) power module increases in power density with high switching speed, parasitic oscillation and localized hot spots caused by power rating degradation become an un-neglected problem in the electric vehicle application. This paper proposes an ultra-low inductance power module integrated with an integrated low temperature co-fired ceramic (LTCC) jet impingement cooling. Ultra-low parasitic inductance leads to low voltage overshoot and low switching losses. The parasitic inductance of a 1200 V/300 A half-bridge SiC power module was reduced to 0.93 nH utilizing wire-bondless connection. To improve power density continuously, a high cooling capability LTCC jet impingement cooler was integrated tightly into the power module with a junction-to-coolant thermal resistance of only 0.06 Kcm^2/W. Compared with the conventional cooling integration structure, the junction-to-coolant thermal resistance was reduced by approximately 71%. The proposed design structure was under development to verify its electrical performance and cooling performance by experiments.**

Keywords—SiC power module, low parasitic inductance, integration, cooling

I. INTRODUCTION

Wide bandgap semiconductor devices, such as SiC, GaN, have been proven to have prominent characteristics of high temperature, high frequency and high blocking voltage in electric vehicles, more electric aircraft, photovoltaic and grid applications [1]-[7]. Lightweight, high power density, and reliability are key goals for power electronics system in electric vehicle applications. However, these goals come at the cost of significant challenges for power module packages. High power density packaging and integration will cause a severe cooling issue in the converter design, which also reduces the reliability of the power electronic systems. Meanwhile, SiC devices are highly sensitive to the parasitic inductance of module packages because of the fast switching speeds. They will lead to high voltage overshoot and parasitic oscillations [2]. Reducing parasitic inductance in the power module, the voltage overshoot, parasitics ringing and switching losses can be reduced effectively, which also benefits its EMI performance and long-term reliability [8]-[13]. Therefore, to fully realize the benefits offered by high-speed and high-temperature SiC devices, it is essential to develop advanced power module packaging architectures with low parasitics and excellent cooling performance.

For the power module, the high parasitic inductance is mainly the result of bonding wires and the power loop length, resulting in high overshoot and parasitic oscillations [1, 2]. Eliminating bonding wires or reducing power loop length leads to lower parasitic inductance [14]. Low parasitic power modules are built by applying the P-cell and N-cell concept [15]. In [16], a flexible printed circuit board based SiC power module was proposed. Benefitting from the flexibility of the PCB and thin PCB substrate, the optimized power loop inductance is 0.79 nH. Flip-chip solder ball interconnection bumped on the chip surface pads effectively reduces the loop parasitics and improves the reliability of the interconnection section. [17, 18].

To combat the thermal challenges raised by improving power density in electric vehicle applications, some novel cooling methods such as spray cooling, jet impingement cooling and microchannels cooling have been presented [19]. Utilizing spray cooing benefits cooler cooling capability improvement at the expense of cooler size increment and coolant pressure drop cased pump power increment. Hirshfeld demonstrated a microchannel cooling with heat fluxes up to 1430 W/cm^2 [20]. 3-D shaped polymer impingement cooler with a 4×4 nozzles array can achieve heat transfer coefficient up to 6.25×104 W/mK with a pump power as low as 0.3 W [21, 22]. With high efficiency jet impingement cooler embedded into the power

This work was supported by the National Science Foundation Engineering Research Center for Power Optimization of Electro Thermal Systems (POETS) under award NSF ERC-1449548.

978-1-7281-9387-8/22/$31.00 ©2022 IEEE

Authorized licensed use limited to: Purdue University. Downloaded on January 16,2023 at 19:51:32 UTC from IEEE Xplore. Restrictions apply.

module, the power converter can achieve a higher power density [23, 24].

In this paper, a wire bondless power module integrated with jet impingement cooler is proposed. The paper's organization is shown as follows: In the first section, wire bondless power module design and development are proposed. In the second section, jet impingement cooler design and development are introduced. In the third section, the integration structure of wire bondless power module and the LTCC jet impingement cooler are analyzed.

II. Wire Bondless Power Module Design And Development

The parasitic inductance of the power module is reduced by both the chip connection inductance and the commutation loop inductance. A solder ball array is applied to minimize the chip connection inductance in the power module. The parasitic inductance of a single solder ball is determined by the bump radius and height. The typical geometric structure of a solder ball is shown in Fig. 1. For a single solder ball, parasitic inductance decreases with bumped radius increases. With consideration for both the manufacturing process, 0.25 mm bumped height solder balls were selected.

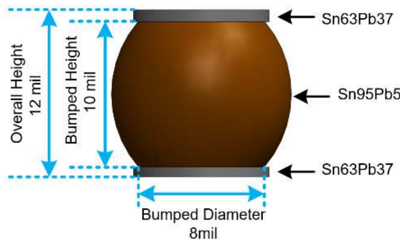

Fig. 1: Solder ball geometric model

The commutation loop inductance is mainly dependent on the mutual inductance cancellation effect and commutation loop length. As shown in Fig. 2(a), the inductance of two parallel conductors with opposite current can be calculated by [9]:

$$L = \frac{u_0 l}{2\pi}\ln(\frac{2l}{t+a}+\frac{1}{2}) - \frac{u_0 l}{2\pi}[\ln\frac{2l}{d}+\frac{1}{2}-2\frac{d}{a}\tan^{-1}\frac{a}{d}-\frac{1}{2}(1-\frac{d^2}{a^2})\ln(1+\frac{d^2}{a^2})] \quad (1)$$

where l is the conductor length, a is the conductor width, t is the conductor thickness and d is the distance between two conductors. As shown in formula (1), while l and d increase, the total inductance will increase, as shown in Fig. 2(b). Self-inductance increases with length l, and the mutual inductance increases with length l and distance d. Meanwhile, the mutual inductance is more sensitive to the distance d [4]. Fig. 2(c) shows that with a specific length, decreasing distance d can reduce total inductance significantly. With a distance lower than 0.4 mm, the commutation loop inductance of the power module can be reduced to under 1 nH.

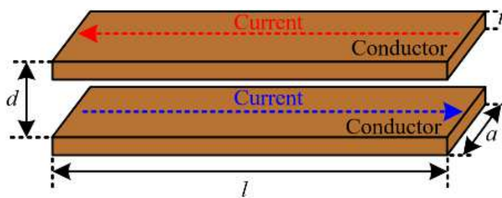

(a) mutual inductance principle

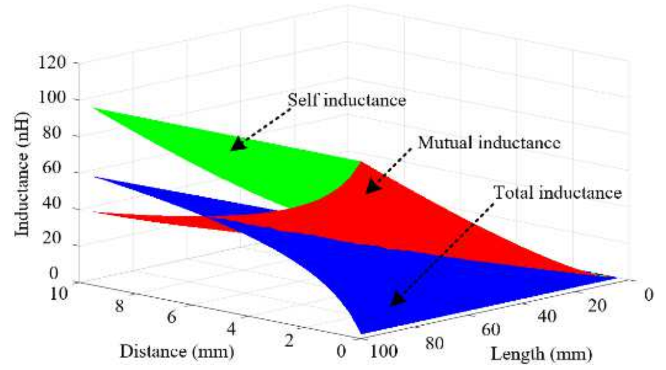

(b) mutual inductance related to distance and length

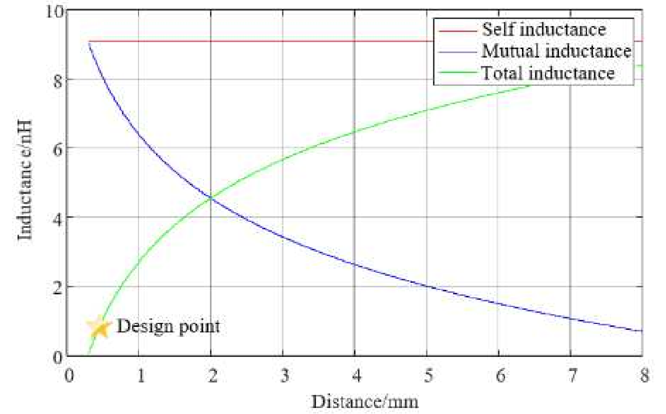

(c) estimated power module design point

Fig. 2: Mutual inductance cancellation effect

The optimized power module structure is proposed with an optimized low-inductance solder ball array connection and commutation loop design, as shown in Fig. 3(a). A laminated terminal design structure reduces the parasitic inductance and improves the current-carrying capability. The laminated busbar can reduce the system's loop parasitics and enhance system compatibility. The gate signal layout is on the top side of the power module. The cooler will be integrated on the bottom side of the power module. The fabricated functional power module is shown in Fig. 3(b). Fig. 3(c) and Fig. 3(d) show the double pulse test platform for power module dynamic performance characterization and test waveform. The overshoot voltage is 70 V under 800 V DC bus voltage.

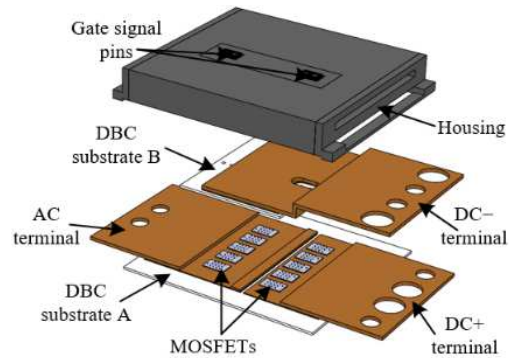

(a) power module structure (exploded view)

Authorized licensed use limited to: Purdue University. Downloaded on January 16,2023 at 19:51:32 UTC from IEEE Xplore. Restrictions apply.

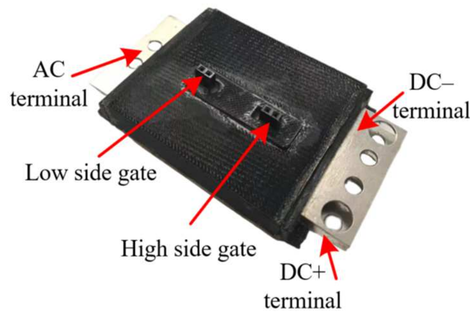

(b) functional power module

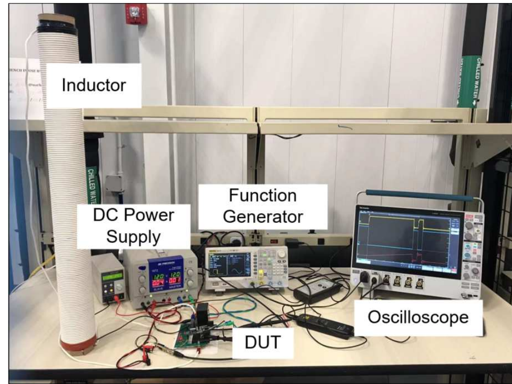

(c) double pulse test platform

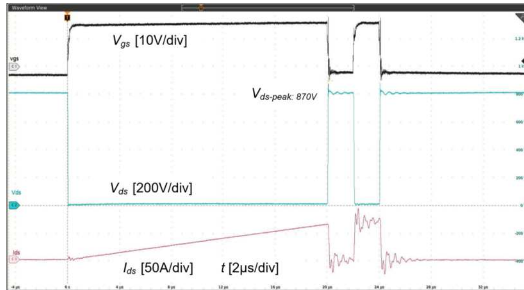

(d) double pulse test waveform

Fig. 3: Proposed power module structure and its dynamic performance test

III. Jet Impingement Cooler Design and Development

A polymer-based impingement jet cooling manifold using an additive manufacturing fabrication process was developed, as shown in Fig. 4. The experimental and CFD modeling studies show that thermal resistance can be reduced to 0.05 cm^{2}K/W for a flow rate of 1 L/min and a pressure drop of 0.3 bar [3].

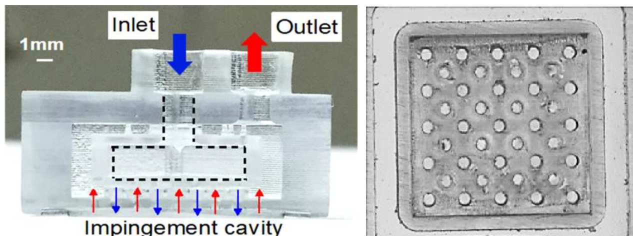

Fig. 4 Cross-section of the 3D printed polymer-based jet impingement jet cooler and bottom view

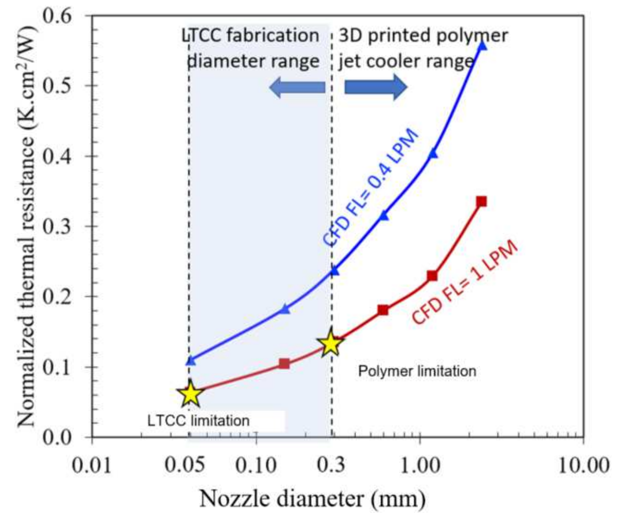

(a) comparison of thermal resistance with nozzle diameter between 3D printed polymer-based and LTCC-based cooler

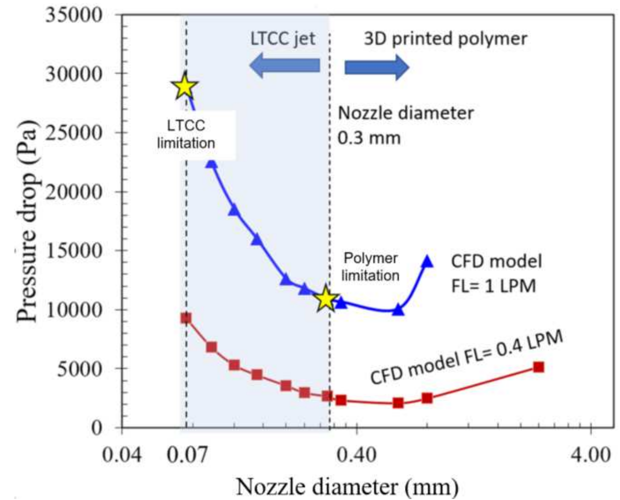

(b) comparison of pressure drop between 3D printed polymer-based and LTCC-based cooler

Fig. 5: Cooling performance comparison between polymer-based and LTCC-based impingement cooler

Compared with the polymer-based structure, the LTCC-based cooler is capable of high-temperature operation with low structure deformation. Meanwhile, the LTCC 50 μm precision manufacture capability provides the potential for a large number of nozzles, which guarantees a more uniform cooling area temperature distribution and low thermal resistance. The comparison of thermal resistance with different nozzle diameters and flow rate between LTCC and 3D printed poly is shown in Fig. 5(a). The thermal resistance of LTCC jet impingement cooling can be reduced by 50% compared to a 3D printed polymer jet cooler. Fig.5 (b) shows the pressure drop comparison between the polymer-based and LTCC-based jet impingement cooler as a function of the nozzle diameter for a constant inlet diameter. A large number of fine nozzles improves thermal performance with lower thermal resistance and more uniform cooling area temperature but at the cost of pressure drop.

Authorized licensed use limited to: Purdue University. Downloaded on January 16,2023 at 19:51:32 UTC from IEEE Xplore. Restrictions apply.

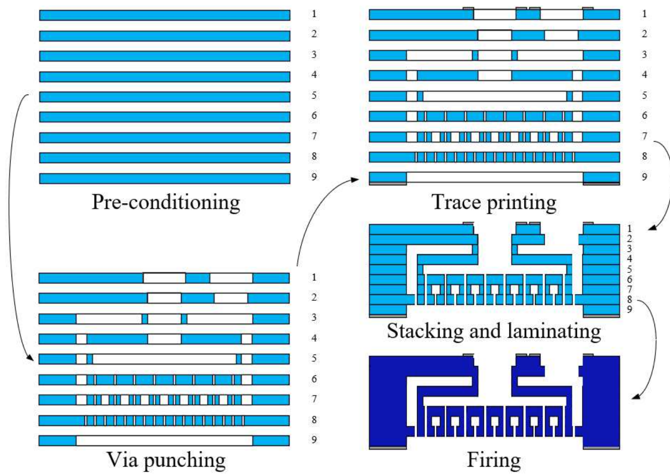

Fig. 6: LTCC-based jet impingement cooler fabrication flow

The LTCC ceramic is composed of multi-layer green tape lamination and firing. The fabrication flow of the LTCC jet impingement cooler is shown in Fig. 6. First, before applying via punching and cutout, the LTCC green tapes are preconditioned at 80 ℃ oven. The preconditioning process is performed to remove the mylar layer from the green tape. Next, the vias are punched by a punching machine with a user-defined punch profile. For the LTCC jet impingement cooler structure, 9 different kinds of green tape are required for the following steps. The thickness of each single green tape is 10 mils. For each kind of layer, multiple layers of green tape are required. Then, after punching each kind of blue tape, DuPont silver-based solderable co-fire paste is used to print the metallization on LTCC. The top side metallization layer is used for soldering to fluid connectors. The bottom side metallization layer is used for soldering the LTCC jet impingement cooler with the power module bottom DBC layer. After the printing process, the silver paste with green tapes is dried inside an oven at 80 ℃ oven. Then, the stacking and lamination process is performed in several steps to guarantee the high uniformity of the laminated structure. Step 1: tape 6, 7 and 8 are laminated at the pressure of 3000 PSI; Step 2: tape 1, 2, 3, and 4 are laminated with a pressure of 2500 PSI; Step 3: the remaining layer are laminated together with previous laminated layers with a pressure of 2000 PSI. Finally, the laminated LTCC structure needs to be fired in an 800 ℃ to 850 ℃ oven with the defined temperature profile over 10 hours.

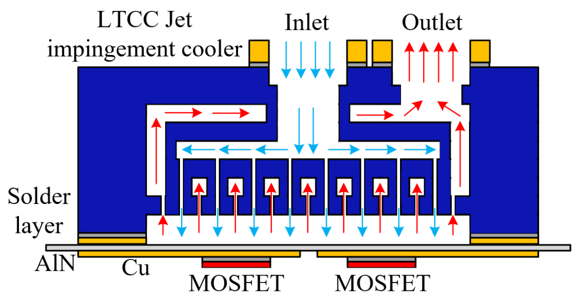

(a) coolant flow loop in LTCC jet impingement cooler

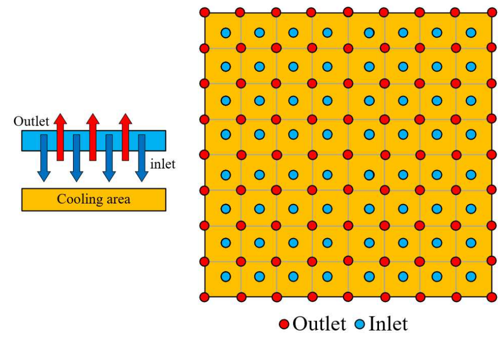

(b) Cooling area nozzles array

Fig. 7: LTCC jet impingement cooler flow loop and cooling area nozzles array

Fig. 7(a) shows the coolant flow loop inside the LTCC jet impingement cooler. The coolant flow splits in different directions and flows through the inlet nozzles, which directly impinging on the backside of the power module AlN layer. Then, after the heat exchange, the coolant flows through the outlet nozzles routing to the outlet port. As shown in Fig. 7(b), the outlet nozzles are designed to layout around the inlet nozzles to minimize the pressure drop of the LTCC jet impingement cooler. Meanwhile, the inlet nozzle surrounded by outlet nozzles' structure performs with uniform temperature distribution.

IV. Jet Impingement Cooler Development and Integration with Power Module

The integration structure of the LTCC jet impingement cooler with the wire bondless power module is shown in Fig. 8(a). The impingement jet cooling structure with alternating feeding and draining jets contains N×N inlet nozzle arrays with outlets surrounded. The jet flow can directly impinge on the backside of the power module. After impinging on the surface, the spent fluid can be efficiently extracted through the outlet nozzle. For the integrated LTCC jet cooling into the power module, the LTCC impinging jet with nozzle diameter of 0.05 mm offers improved thermal performance of 0.06 cm^2K/W for a flow rate of 1 L/min and pressure drop of 0.3 bar.

The jet impingement cooler was bonded to the DBC AlN layer with no leakage of fluid, which guarantees the cooling performance of the jet impingement cooler. By eliminating the baseplate layer, the DBC bottom copper layer and two solder layers, the junction-to-coolant thermal resistance achieved is 0.06 cm^2K/W. Compared with the conventional cooler bonding to power module baseplate structure, the thermal resistance is reduced by approximately 71% as shown in Fig. 8(b).

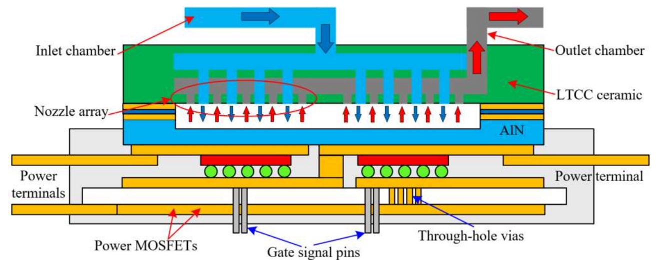

Authorized licensed use limited to: Purdue University. Downloaded on January 16,2023 at 19:51:32 UTC from IEEE Xplore. Restrictions apply.

(a) proposed schematic of the LTCC jet impingement cooler with wire bondless power module

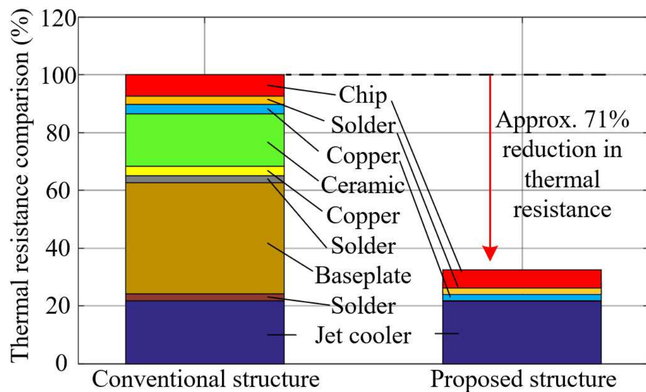

(b) thermal resistance comparison with conventional structure

Fig. 8: Proposed integration structure and junction-to-coolant thermal resistance comparison

Conclusions

In this paper, an ultra-low inductance power module with integrated LTCC jet impingement cooling is proposed. The fabrication process of the LTCC impingement cooler has been developed. The optimized parasitic inductance of a 1200 V/300 A half-bridge SiC power module was reduced to 0.93 nH by simulation. The overshoot voltage of the proposed power module is 70 V with an 800 V DC bus voltage. A high cooling capability LTCC jet impingement cooler was integrated tightly into the power module with a thermal resistance low to 0.06 Kcm^2/W. Compared with the conventional cooling integration structure, the junction-to-coolant thermal resistance was reduced by approximately 71%.

References

[1] R. Alizadeh and H. Alan Mantooth, "A Review of Architectural Design and System Compatibility of Power Modules and Their Impacts on Power Electronics Systems," in *IEEE Transactions on Power Electronics*, vol. 36, no. 10, pp. 11631-11646, Oct. 2021, doi: 10.1109/TPEL.2021.3068760.

[2] S. Seal, M. D. Glover, and H. Alan. Mantooth, "3-D Wire Bondless Switching Cell Using Flip-Chip-Bonded Silicon Carbide Power Devices," in *IEEE Transactions on Power Electronics*, vol. 33, no. 10, pp. 8553-8564, Oct. 2018.

[3] Z. Zeng, X. Zhang, F. Blaabjerg, H. Chen and T. Sun, "Stepwise Design Methodology and Heterogeneous Integration Routine of Air-Cooled SiC Inverter for Electric Vehicle," in *IEEE Transactions on Power Electronics*, vol. 35, no. 4, pp. 3973-3988, April 2020, doi: 10.1109/TPEL.2019.2937135.

[4] F. Guo, T. Yang, A. M. Diab, S. S. Yeoh, S. Bozhko and P. Wheeler, "An Enhanced Virtual Space Vector Modulation Scheme of Three-Level NPC Converters for More-Electric-Aircraft Applications," in *IEEE Transactions on Industry Applications*, vol. 57, no. 5, pp. 5239-5251, Sept.-Oct. 2021, doi: 10.1109/TIA.2021.3085798.

[5] Z. Zeng, W. Shao, H. Chen, B. Hu, W. Chen, H. Li, L. Ran, "Changes and challenges of photovoltaic inverter with silicon carbide device," *Renewable and Sustainable Energy Reviews*, vol. 78, pp. 624-639, 2017. doi: 10.1016/j.rser.2017.04.096

[6] X. Li, Y. Chen, Y. Wu, H. Chen, W. Weber, A. Nasiri, R. Cuzner, Y. Zhao, H. A. Mantooth, "High Voltage SiC Power Module Optimized for Low Parasitics and Compatible System Interface," *2022 IEEE Applied Power Electronics Conference and Exposition (APEC)*, 2022, pp. 999-1003, doi: 10.1109/APEC43599.2022.9773726.

[7] X. Li, H. Jiang, B. Hu, H. Chen, Z. Zeng, L. Ran, P. Mawby, "Electro-Thermal Limited Switching Frequency for Parallel Diodes," *2018 IEEE Energy Conversion Congress and Exposition (ECCE)*, 2018, pp. 4692-4698, doi: 10.1109/ECCE.2018.8557614.

[8] N. Jia, X. Tian, L. Xue, H. Bai, L. M. Tolbert, H. Cui, "In-package Common-Mode Filter for GaN Power Module with Improved Radiated EMI Performance, " *2022 IEEE Applied Power Electronics Conference and Exposition (APEC)*, 2022, pp. 974-979, doi: 10.1109/APEC43599.2022.9773764.

[9] A. I. Emon, Z. Yuan, A. B. Mirza, A. Deshpande, M. U. Hassan and F. Luo, "1200 V/650 V/160 A SiC+Si IGBT 3L Hybrid T-Type NPC Power Module With Enhanced EMI Shielding," in *IEEE Transactions on Power Electronics*, vol. 36, no. 12, pp. 13660-13673, Dec. 2021, doi: 10.1109/TPEL.2021.3089578.

[10] A. B. Mirza, A. I. Emon, S. S. Vala and F. Luo, "Noise Immune Cascaded Gate Driver Solution for Driving High Speed GaN Power Devices," *2021 IEEE Energy Conversion Congress and Exposition (ECCE)*, 2021, pp. 5366-5371, doi: 10.1109/ECCE47101.2021.9595515.

[11] Y. Chen, L. Du and J. He, "Online Diagnosis and Ride-Through Operation for Cascaded H-Bridge Converter Based STATCOM With a Single Open-Circuit IGBT," in *IEEE Transactions on Industrial Electronics*, vol. 69, no. 8, pp. 7549-7559, Aug. 2022, doi: 10.1109/TIE.2021.3104578.

[12] X. Li, Z. Zeng, H. Chen, W. Shao and L. Ran, "Comparative Evaluations and Failure Modes of Wire-Bonding Packaged SiC, Si, and Hybrid Power Modules," *2018 1st Workshop on Wide Bandgap Power Devices and Applications in Asia (WiPDA Asia)*, 2018, pp. 16-22, doi: 10.1109/WiPDAAsia.2018.8734535.

[13] X. Du, Y. Wei, A. Stratta, L. Du, V. S. Machireddy and A. Mantooth, "A Four-level Active Gate Driver with Continuously Adjustable Intermediate Gate Voltages," *2022 IEEE Applied Power Electronics Conference and Exposition (APEC)*, 2022, pp. 1379-1386, doi: 10.1109/APEC43599.2022.9773689.

[14] C. Zheng, Y. Yao, D. Boroyevich, K. D. T. Ngo, P. Mattavelli, and K. Rajashekara, "A 1200-V, 60-A SiC MOSFET Multichip Phase-Leg Module for High-Temperature, High-Frequency Applications," *IEEE Transactions on Power Electronics*, vol. 29, pp. 2307-2320, 2014.

[15] S. Li, L. M. Tolbert, F, and F. Z. Peng, "Stray Inductance Reduction of Commutation Loop in the P-cell and N-cell-Based IGBT Phase Leg Module," *IEEE Transactions on Power Electronics*, vol. 29, pp. 36163624, 2014.

[16] C. Chen, Z. Huang, L. Chen, Y. Tan, Y. Kang and F. Luo, "Flexible PCB-Based 3-D Integrated SiC Half-Bridge Power Module With Three-Sided Cooling Using Ultralow Inductive Hybrid Packaging Structure," in *IEEE Transactions on Power Electronics*, vol. 34, no. 6, pp. 5579-5593, June 2019, doi: 10.1109/TPEL.2018.2866404.

[17] H. Chen, T. Wei, Y. Chen, X. Li, N. Li, Q. Zhu, S. Hazra, Y. Zhao, M. P. Gupta, M. Asheghi, Y. Lu, K. Goodson, H. A. Mantooth, "Feasibility Design of Tight Integration of Low Inductance SiC Power Module with Microchannel Cooler," *2022 IEEE Applied Power Electronics Conference and Exposition (APEC)*, 2022, pp. 962-965, doi: 10.1109/APEC43599.2022.9773698.

[18] H. Chen, M. Hossain, D. G. Castillo, X. Li, A. Wallace, Y. Chen, H. A. Mantooth, "Design and Optimization of SiC MOSFET Wire Bondless Power Modules," *2020 IEEE 9th International Power Electronics and Motion Control Conference (IPEMC2020-ECCE Asia)*, 2020, pp. 725-728, doi: 10.1109/IPEMC-ECCEAsia48364.2020.9368008.

[19] R. Whitt, D. Huitink, A. Emon, A. Deshpande, and F. Luo, "Thermal and Electrical Performance in High-Voltage Power Modules With Nonmetallic Additively Manufactured Impingement Coolers," in *IEEE Transactions on Power Electronics*, vol. 36, no. 3, pp. 3192-3199, March 2021.

[20] H. Hirshfeld, I. Silverman, A. Arenshtam, D. Kijel and A. Nagler, "High heat flux cooling of accelerator targets with micro-channels", *Nucl. Instrum. Methods Phys. Res. Sect. A-Accel. Spectrometers Detect. Assoc. Equip.*, vol. 562, no. 2, pp. 903-905, Jun. 2006.

Authorized licensed use limited to: Purdue University. Downloaded on January 16,2023 at 19:51:32 UTC from IEEE Xplore. Restrictions apply.

[21] T. Wei, H. Oprins, V. Cherman, J. Qian, I. Wolf, E. Beyne and M. Baelmans, "High-Efficiency Polymer-Based Direct Multi-Jet Impingement Cooling Solution for High-Power Devices," in *IEEE Transactions on Power Electronics*, vol. 34, no. 7, pp. 6601-6612, July 2019, doi: 10.1109/TPEL.2018.2872904.

[22] T. Wei, H. Oprins, V. Cherman, E. Beyne and M. Baelmans, "Low-Cost Energy-Efficient On-Chip Hotspot Targeted Microjet Cooling for High-Power Electronics," in *IEEE Transactions on Components, Packaging and Manufacturing Technology*, vol. 10, no. 4, pp. 577-589, April 2020, doi: 10.1109/TCPMT.2019.2948522.

[23] T. Wei, H. Oprins, V. Cherman, S. Yang, I. Wolf, E. Beyne and M. Baelmans, "Experimental Characterization of a Chip-Level 3-D Printed Microjet Liquid Impingement Cooler for High-Performance Systems," in *IEEE Transactions on Components, Packaging and Manufacturing Technology*, vol. 9, no. 9, pp. 1815-1824, Sept. 2019, doi: 10.1109/TCPMT.2019.2905610.

[24] T. Wei, H. Oprins, V. Cherman, Z. Yang, K. Rivera, G. Plas, B. J. Pawlak, L. England, E. Beyne and M. Baelmans, "Experimental and Numerical Study of 3-D Printed Direct Jet Impingement Cooling for High-Power, Large Die Size Applications," in *IEEE Transactions on Components, Packaging and Manufacturing Technology*, vol. 11, no. 3, pp. 415-425, March 2021, doi: 10.1109/TCPMT.2020.3045113.

Authorized licensed use limited to: Purdue University. Downloaded on January 16,2023 at 19:51:32 UTC from IEEE Xplore. Restrictions apply.